Journal of Hazardous Materials 497 (2025) 139696

Contents lists available at ScienceDirect

Journal of Hazardous Materials

journal homepage: www.elsevier.com/locate/jhazmat

Microplastic exposure aggravates pneumococcus-induced inflammation in macrophages by activating ferroptosis

Ko-Wei Chang [a,b,c,1], Jo-Tsen Chen [d,e,1], Chun-Ning Chuang [d,f], Dang Thi Thanh Thao [d], Yu-Tsen Huang [d], Hui-Yu Wu [d], Ming-Ling Kuo [d,g], Kuo-Chin Kao [a,h], Cheng-Hsun Chiu [d,g], Chih-Ho Lai [d,g,i,j,k,*]

[a] Department of Thoracic Medicine, Chang Gung Memorial Hospital at Linkou, Taoyuan, Taiwan
[b] Graduate Institute of Clinical Medical Sciences, College of Medicine, Chang Gung University, Taoyuan, Taiwan
[c] School of Medicine, National Tsing Hua University, Hsinchu, Taiwan
[d] Department of Microbiology and Immunology, Graduate Institute of Biomedical Sciences, College of Medicine, Chang Gung University, Taoyuan, Taiwan
[e] Department of Laboratory Medicine, Chang Gung Memorial Hospital at Linkou, Taoyuan, Taiwan
[f] Department of Pathology & Laboratory Medicine, Taichung Veterans General Hospital, Taichung, Taiwan
[g] Division of Allergy, Asthma, and Rheumatology, Molecular Infectious Disease Research Center, Department of Pediatrics, Chang Gung Memorial Hospital at Linkou, Taoyuan, Taiwan
[h] Department of Respiratory Therapy, College of Medicine, Chang Gung University, Taoyuan, Taiwan
[i] Department of Microbiology and Immunology, Department of Medical Research, China Medical University and Hospital, Taichung, Taiwan
[j] Department of Nursing, Asia University, Taichung, Taiwan
[k] Research Center for Emerging Viral Infections, Institute of Immunology and Translational Medicine, Chang Gung University, Taoyuan, Taiwan

HIGHLIGHTS

- MP exposure impairs macrophage phagocytosis and bacterial clearance.
- MPs exacerbate pneumococcal inflammation via CCL2-mediated PI3K/Akt activation.
- Co-exposure to MPs and pneumococcus elevates ROS and disrupts iron homeostasis.
- MPs trigger macrophage dysfunction and ferroptosis, aggravating lung infections.

GRAPHICAL ABSTRACT

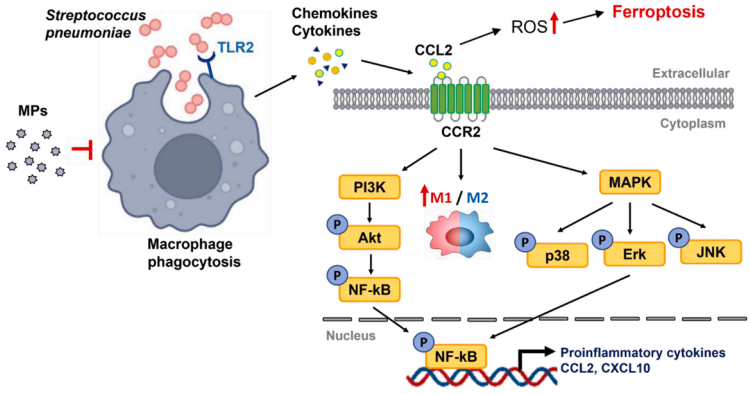

ARTICLE INFO

Keywords:
Microplastics

ABSTRACT

Microplastics (MPs) are ubiquitous environmental pollutants posing serious concerns owing to their potential health implications. MPs exert detrimental effects via the plastic particles, MP-bound chemicals, and MP-carrying

* Corresponding author at: Department of Microbiology and Immunology, Graduate Institute of Biomedical Sciences, College of Medicine, Chang Gung University, Taoyuan, Taiwan.
E-mail address: chlai@mail.cgu.edu.tw (C.-H. Lai).
[1] Equal contribution to the first author

https://doi.org/10.1016/j.jhazmat.2025.139696
Received 2 April 2025; Received in revised form 19 August 2025; Accepted 28 August 2025
Available online 29 August 2025

Pneumococcus
Macrophage
Inflammatory response
CCL2
Ferroptosis

pathogens. *Streptococcus pneumoniae* (pneumococcus) is a major pathogen causing bacterial pneumonia and respiratory inflammation. However, specific immune responses of macrophages to pneumococcus under MP exposure remain unclear. In this study, we aimed to investigate the mechanisms by which MPs inhibit macrophage functions, bacterial clearance, and inflammation during pneumococcal infection. Our results showed that MP exposure significantly impaired macrophage phagocytosis and inhibited pneumococcal engulfment. Furthermore, MPs synergistically enhanced C-C motif chemokine ligand 2 (CCL2) production via the phosphoinositide 3-kinase/protein kinase B (PI3K/Akt) and mitogen-activated protein kinase/extracellular signal-regulated kinase (MAPK/ERK) pathways, promoting M1 macrophage polarization and activating the ferroptosis pathway upon pneumococcal infection. Understanding the roles of MPs in the exacerbation of macrophage-driven inflammation will facilitate the development of new strategies to manage and treat pneumococcus-induced pulmonary diseases.

1. Introduction

Microplastics (MPs), defined as plastic particles ranging from 1 μm to 5 mm in diameter, are emerging environmental pollutants posing a serious threat to human health owing to their increasing prevalence in almost all ecosystems [1]. Based on their building chemical composition, MPs are classified into various types, including polyethylene (PE)-, polystyrene (PS)-, polypropylene (PP)-, polyvinyl chloride (PVC)-, and polyethylene terephthalate (PET)-based MPs [1]. Among them, PS-based MPs are most commonly used in research due to their defined size and easily accessible surface chemistry, which are highly important for particle–cell interactions [2].

Streptococcus pneumoniae (also referred to as pneumococcus) is among the most common pathogens causing respiratory tract infections [3]. Pneumococcus frequently colonizes the upper respiratory tract of humans, and this asymptomatic colonization can progress to invasive diseases and conditions, such as sepsis, meningitis, and community-acquired pneumonia [4]. Alveolar macrophages are crucial for the early immune responses to pulmonary infections via pathogen phagocytosis [5,6]. In addition to directly killing the invading microorganisms, macrophages secrete various inflammatory cytokines and chemokines, including the tumor necrosis factor (TNF)-α, interleukin (IL)-6, IL-1α/β, C-C motif chemokine ligand 2 (CCL2), and C-X-C motif chemokine ligand 10 (CXCL10), which are involved in the pathogenesis and regulation of pneumococcal infection [7,8]. Additionally, both M1- and M2-polarized macrophages play vital roles in regulating pneumococcal pneumonia [9].

Exposure to air pollutant particles induces lung and systemic inflammation and exacerbates infectious diseases [10]. Among these pollutants, airborne MPs pose a unique threat due to their ability to leach heavy metals, chemical substances, and other harmful contaminants absorbed from the environment, increasing their toxicity to humans [11,12]. The detrimental effects of MPs on immune cells have been reported. For instance, MPs are strongly bound to and engulfed by neutrophils, enhancing the pro-inflammatory activity and cell death-related functions of neutrophils through the Toll-like receptor pathway [13]. Similarly, MPs are internalized by macrophages through scavenger receptor-mediated phagocytosis, leading to various immunomodulatory effects [14]. In RAW264.7 cells, MPs have been shown to disrupt mitochondrial function and induce the generation of reactive oxygen species (ROS) [15]. In THP-1-derived macrophages, MP exposure impairs phagocytic activity and causes DNA damage, indicating a weakened innate immune response [16]. Furthermore, studies using primary peritoneal macrophages have demonstrated MP-induced cytotoxicity and polarization toward a pro-inflammatory phenotype [17]. Collectively, these findings suggest that MPs directly interfere with immune defenses and may exacerbate microbial infections. However, despite growing interest in MP toxicity, limited research has addressed how MPs influence macrophage responses in the context of bacterial infections.

Pro-inflammatory cytokines regulate intracellular iron homeostasis and redox balance, triggering various inflammation-related signaling pathways associated with ferroptosis, including the nuclear factor kappa-light-chain-enhancer of activated B cells (NF-κB), inflammasome, and mitogen-activated protein kinase (MAPK) pathways [18]. Ferroptotic cells contribute to inflammatory responses and disease progression by promoting macrophage recruitment and chemotaxis via CCL2 [19]. CCL2 activity is influenced by macrophage polarization toward the pro-inflammatory M1 phenotype [20]. MP exposure activates ROS and initiates ferroptosis [21]. MP-induced ROS production promotes biofilm formation and enhances bacterial virulence and antibiotic resistance [22]. Despite these findings, the specific roles of ferroptosis and oxidative stress in exacerbating MP- and pneumococcus-induced macrophage inflammation remain poorly understood. This study aims to elucidate the detailed mechanisms by which MPs impair macrophage-mediated immune responses during pneumococcal infection, with a particular focus on macrophage functions.

2. Materials and methods

2.1. Characterization of polystyrene-based microplastics (PS-MPs)

PS-MPs with a diameter of less than 0.1 μm (product no. 90517) were purchased from Sigma-Aldrich (St. Louis, MO, USA). After gentle mixing, 2 μL of a 2 % polystyrene aqueous particle solution was pipetted and evenly spread onto an agar plate. The MP suspensions were air-dried at room temperature overnight, then coated with gold using an ion sputter coater (E-1010, Hitachi, Japan). Images were taken using a field-emission scanning electron microscope (FE-SEM) (JSM 7500 F, JEOL, Tokyo, Japan).

2.2. Cell culture

RAW264.7 cells (ATCC TIB-71), a murine macrophage cell line, were obtained from the American Type Culture Collection (ATCC, Manassas, VA, USA). Given their widespread use in bacterial infection models, RAW264.7 cells were employed for the subsequent experiments in this study (Figure S1). The cells were cultured in Dulbecco's Modified Eagle Medium (DMEM, Invitrogen, Carlsbad, CA, USA) supplemented with 10 % heat-inactivated fetal bovine serum (FBS). Cells were maintained at 37°C in a humidified incubator with 5 % CO_2.

2.3. Bacterial culture

The pneumococcal strain TIGR4 (ATCC BAA-334) was kindly provided by Professor Cheng-Hsun Chiu (Chang Gung Memorial Hospital at Linkou, Taoyuan, Taiwan) [23]. The bacteria were grown on blood agar plates (Becton Dickinson, Sparks, MD, USA) and cultured at 37°C in a 5 % CO_2 atmosphere, as described previously [24]. For infection experiments, bacteria were refreshed in Todd Hewitt Broth (Becton Dickinson) until an OD_{600} of 0.6 was reached before proceeding with subsequent experiments.

2.4. Cell viability assay

RAW264.7 cells (1×10^5) were plated in 96-well plates and exposed

to various concentrations of MPs for 24 h. Cells were incubated at 37°C with 0.5 mg/mL 3-(4,5-dimethylthiazol-2-yl)-2,5-diphenyltetrazolium bromide (MTT) solution for 3 h. The formazan crystals were dissolved in isopropanol, and the absorbance at 570 nm was measured using a spectrophotometer (Bio-Rad, Hercules, CA, USA). Cell viability was expressed as a percentage relative to the group untreated with MPs.

2.5. Phagocytosis assay

The effect of MPs on macrophage phagocytic activity was assessed using a Phagocytosis Assay Kit (IgG FITC) (#500290, Cayman Chemical, Ann Arbor, MI, USA), following the manufacturer's instructions. Briefly, RAW264.7 cells (2×10^6) were seeded onto coverslips and treated with MPs at concentrations of 0, 20, 100, and 1000 μg/mL for 6 h. Macrophages were then incubated with fluorescein isothiocyanate (FITC)-labeled latex beads coated with rabbit IgG for 3 h at 37°C. After incubation, cells were fixed with 2 % paraformaldehyde for 40 min and stained with Hoechst 33342 (AAT Bioquest, Sunnyvale, CA, USA) for 30 min. The stained cells were mounted on coverslips and visualized using a Laser Scanning Confocal Microscope (LSM780, ZEISS, Oberkochen, Germany).

2.6. Bacterial internalization assay

A gentamicin protection assay was performed to assess the impact of MPs on the internalization of bacteria by macrophages. RAW264.7 cells were treated with MPs at concentrations of 0, 20, 100, and 1000 μg/mL for 24 h, followed by infection with pneumococci at a multiplicity of infection (MOI) of 10 for 4 h. To eliminate extracellular bacteria, infected cells were treated with 100 μg/mL gentamicin for 1.5 h. Cells were then lysed with 0.1 % Triton X-100 for 30 min. The lysates were serially diluted and plated on blood agar plates. Colony-forming units (CFU) were enumerated to determine the internalized bacteria.

2.7. Cytokine array analysis

Expression levels of cytokines were determined by a Proteome Profiler Mouse Cytokine Array kit (#ARY006, R&D Systems, Minneapolis, MN, USA). The experimental settings were divided into two groups, including Sp (pneumococci-only treated cells with MOI = 10 for 4 h), and MPs + Sp (cells were primarily treated with MPs of 20 μg/mL, then infected with pneumococci with MOI = 10 for 4 h). The chromogenic detection of membranes was used with AzureSpot Analysis chromogenic detection software (Azure Biosystems, Dublin, CA, USA) of the Azure c400 system. The pixel density of each dot was analyzed by UN-SCAN-IT gel Analysis Software (Silk Scientific, Provo, UT, USA). After that, the level of each cytokine was determined as the average signal of the duplicate spots subtracted from the background signal. The relative changes in cytokine levels between groups were normalized to total protein concentration, and the fold changes were calculated using $\log_2$.

2.8. RNA extraction and quantitative real-time PCR (qRT-PCR)

Total RNA was isolated from cells using a PureLink™ RNA Mini kit (#12183018 A, Thermo Fisher Scientific, Rockford, IL, USA) according to the manufacturer's protocol, followed by analyzing the quantity and quality of extracted RNA using a NanoDrop spectrophotometer (Thermo Fisher Scientific, Rockford, IL, USA) and an Agilent 2100 Bioanalyzer (Agilent Technologies, Santa Clara, CA, USA) [25]. RNA was reversely transcribed into cDNA using an iScript cDNA Synthesis kit (#1708890, Bio-Rad, Hercules, CA, USA). The primer sequences used in this study are shown in Table 1 and subjected to qRT-PCR analysis. qRT-PCR analysis was set up with SYBR Green I Master Mix using a model 7900 Sequence Detector System (Applied Biosystems, Foster, CA, USA), which was conducted by following the manufacturer's instructions. Thermal cycling conditions were as follows: an initial denaturation at 95°C for 10 min, followed by 35 cycles of denaturation at 95°C for 10 sec and annealing/extension at 60°C for 1 min. mRNA expression levels were normalized to the control group and quantified using the $2^{-\Delta\Delta Ct}$ method.

Table 1
Primers used for quantitative real-time PCR analysis[†].

Gene	Primer	Sequence
CCL2	Forward	5'-GCATCCACGTGTTGGCTCAG- 3'
	Reverse	5'-TTCTTGGGGTCAGCACAGAC- 3'
CCR2	Forward	5'-TCTTCCTGCTCACATTACCA- 3'
	Reverse	5'-GCCAAGTACCTATCAATTGT- 3'
CXCL10	Forward	5'-CCAAGTGCTGCCGTCATTTTC- 3'
	Reverse	5'-GGCTCGCAGGGATGATTTCAA- 3
CXCR3	Forward	5'-TACCTTGAGGTTAGTGAACGTCA- 3'
	Reverse	5'-CGCTCTCGTTTTCCCCATAATC- 3'
ICAM−1	Forward	5'- CAATTTCTCATGCCGCACAG- 3'
	Reverse	5'- AGCTGGAAGATCGAAAGTCCG- 3'
IL−1ra	Forward	5'- AGTACTGCCGAGGCCTGTAATAA- 3'
	Reverse	5'- TTGTTCCTCAGGCCCCAAT- 3'
GM-CSF	Forward	5'-GAGCATGTGAATGCCATCCAGGAG- 3'
	Reverse	5'-CTCCTGGACTGGCTCCCAGCAGTCAAA- 3'
TLR2	Forward	5' -TCTGGGCAGTCTTGAACATTT- 3'
	Reverse	5' -AGAGTCAGGTGATGGATGTCG- 3'
CD80	Forward	5' -AACTCGCATCTACTGGCAAAAGGAGAA- 3'
	Reverse	5' -GGGAAACTGTTGTGTTGATGGCATTTA- 3'
iNOS	Forward	5' -GACATTACGACCCCTCCCAC- 3'
	Reverse	5' -GCACATGCAAGGAAGGGAAC- 3'
CD163	Forward	5' -GGCTAGACGAAGTCATCTGCAC- 3'
	Reverse	5' -CTTCGTTGGTCAGCCTCAGAGA- 3'
CD206	Forward	5' -CTAACTGGGGTGCTGACGAG- 3'
	Reverse	5' -GGCAGTTGAGGAGGTTCAGT- 3'
GAPDH	Forward	5' -ATGGTGAAGGTCGGTGTGAA- 3'
	Reverse	5' -CGCTCCTGGAAGATGGTGAT- 3'

[†]qRT-PCR was performed using SYBR Green I Master Mix. Relative mRNA expression levels were normalized to the control group and calculated using the $2^{-\Delta\Delta Ct}$ method. Data are presented as fold change relative to control.

2.9. Enzyme-linked immunosorbent assay (ELISA)

RAW264.7 cells were either untreated or treated with 20 μg/mL MPs for 24 h, followed by uninfected or infected with pneumococci (MOI = 10) for 4 h. The expression levels of CCL2 and CXCL10 were determined using a Duoset ELISA kit (#DY479 and #DY466, R&D Systems, Minneapolis, MN, USA).

2.10. SDS-PAGE and western blot analysis

RAW 264.7 cells were treated or untreated with MPs (20 μg/mL) for 24 h, followed by infection with pneumococci (MOI = 10) for 4 h. Cells were lysed with RIPA buffer containing protease and phosphatase inhibitors (Roch, Indianapolis, IN, USA). Protein concentrations were determined by Bicinchoninic Acid (BCA) Protein Assay (#23225, Pierce™ BCA Protein Assay kit, Thermo Fisher Scientific, Rockford, IL, USA). Cell lysates were resolved by SDS-PAGE and transferred onto polyvinylidene difluoride membranes (Millipore, Billerica, MA, USA). The membranes were blocked by blocking buffer (containing 5 % bovine serum albumin (BSA) and 0.1 % Tween 20 in TBS) for 1 h and then incubated overnight with primary antibodies. The primary antibodies used in the study were: anti-PI3K (#4292; 1:1000), anti-p-Akt (#4691; 1:1000), anti-t-Akt (#4060; 1:1000), anti-p-NF-κB p65 (#3033; 1:1000), anti-p-p38 (#4511; 1:1000), anti-t-p38 (#8690; 1:1000), anti-p-ERK1/2 (#4370; 1:1000), anti-t-ERK1/2 (#4695; 1:1000), anti-p-JNK1/2 (#9251; 1:1000), anti-JNK1/2 (#9252; 1:1000), and anti-FTH1 (#4393; 1:1000), which were purchased from Cell Signaling Technology (Beverly, MA, USA). Antibodies specific to NF-κB p65 (GTX107678; 1:1000) and p53 (GTX102090; 1:1000) were purchased from GeneTex (Irvine, CA, USA). Antibodies against Xct (ab175186; 1:1000) and glutathione peroxidase 4 (GPX4) (ab125066; 1:1000) were purchased from Abcam (Cambridge, UK). Antibodies specific to NCOA4 (sc373739;

1:1000) and β-actin (sc48772; 1:5000) were obtained from Santa Cruz Biotechnology (Santa Cruz, CA, USA). Horseradish peroxidase (HRP)-conjugated goat anti-rabbit/mouse IgG (Millipore) were used as secondary antibodies, and the proteins of interest were detected by ECL Western Blotting Detection Reagents (GE Healthcare, Piscataway, NJ, USA), and measured using Azure c400 system with AzureSpot Analysis Software (Azure Biosystems, Dublin, CA, USA).

2.11. Luciferase activity assay

RAW 264.7 cells (6×10^4) were seeded into 24-well plates and co-transfected with Renilla and NF-κB luciferase reporter genes using jetPRIME (#101000001, Polyplus-transfection, Illkirch-Graffenstaden, France) according to the manufacturer's instructions. Cells were untreated or treated with 20 μg/mL MPs for 24 h, followed by infection with pneumococci (MOI = 10) for an additional 4 h. The transfected cells were lysed and analyzed with the Dual-Luciferase Reporter Assay System (#E1910, Promega, Madison, WI, USA). The luminescence was detected by using SpectraMax® iD3 Multi-Mode Microplate Readers (Molecular Devices LLC, San Jose, CA, USA).

2.12. Intracellular iron measurement

RAW264.7 cells (2×10^5) were seeded into 6-well plates and exposed to 20 μg/mL MPs for 24 h, followed by pneumococcal challenge (MOI = 10) for 6 h. The cells were stained with 1 μmol/L FerroOrange (#F374, DojinDo, Japan) and incubated for 30 min in a 37°C incubator equilibrated with 5 % CO_2 to measure intracellular iron concentration. Ferric carrier proteins dissociated ferric iron (Fe^{3+}) in the intracellular reductive environment, and the ferrous ion (Fe^{2+}) reacted with FerroOrange probes to produce a stable-colored complex. The fluorescence intensity was observed under a fluorescence microscope (Zeiss AxioVert 135; Carl Zeiss, Oberkochen, Germany).

2.13. ROS production assay

Intracellular ROS production was detected using dihydrorhodamine 123 (DHR 123) (#D23806, Invitrogen, Thermo Fisher Scientific, Rockford, IL, USA). DHR 123 is a nonfluorescent membrane-permeable probe, which fluoresces when oxidized to cationic rhodamine 123 in the mitochondria. RAW264.7 cells (2×10^5) were plated in 6-well plates and exposed to 20 μg/mL MPs for 24 h, followed by pneumococcal infection (MOI = 10) for 2 h. After the treatment, 10 μM DHR 123 was added to the cells and incubated for 30 min at 37°C. The fluorescence intensity was analyzed by flow cytometry.

2.14. Lipid peroxidation assay

Lipid ROS production was assessed using BODIPY-C11 (#D3861, Invitrogen, Thermo Fisher Scientific, Rockford, IL, USA), a fluorescent probe for detecting lipid peroxidation in cellular membranes. RAW264.7 cells (2×10^5) were seeded into 6-well plates and pretreated with 5 μg/mL ferrostatin-1 (Fer-1), a potent ferroptosis inhibitor, for 1 h before exposure to MPs and subsequent pneumococcal challenge. After treatment, the cells were incubated with 10 μM BODIPY-C11 for 30 min at 37°C. Fluorescence intensity was then analyzed by flow cytometry (Becton Dickinson, San Jose, CA, USA).

2.15. Ferrostatin-1 treatment and cell death assay

RAW264.7 cells were pretreated with ferrostatin-1 (5 μg/mL) for 1 h, followed by exposure to MPs for 24 h and subsequent infection with pneumococci (MOI = 10) for 3 h. The release of lactate dehydrogenase (LDH) was measured using the CytoTox 96® Non-Radioactive Cytotoxicity Assay Kit (#G1780, Promega, Madison, WI, USA). Briefly, 25 μL of culture supernatant from each well was collected and mixed with an equal volume of the provided substrate mixture. The reaction was carried out at room temperature for 30 min in the dark and terminated by adding the stop solution. Absorbance was measured at 490 nm using a microplate reader (SpectraMax iD3, Molecular Devices, CA, USA). Cell cytotoxicity was calculated as follows: Cytotoxicity (%) = (Sample – Blank) / (Positive Control – Blank) × 100.

2.16. Statistical analysis

Prior to statistical analysis, the Shapiro–Wilk test was performed to assess the normality of data distribution, and the Brown–Forsythe test was used to evaluate the homogeneity of variances. Based on these assessments, either parametric or non-parametric tests were selected accordingly. For statistical validation, both unpaired Student's *t*-test and one-way ANOVA were conducted to compare means between groups, serving to cross-validate the consistency of significance. When comparing two groups, Student's *t*-test was applied; for comparisons involving more than two groups, one-way ANOVA followed by Tukey's post hoc test was used. All statistical analyses were performed using Prism 8 (GraphPad Software, La Jolla, CA, USA). Statistical significance was defined as $^*p < 0.05$, $^{**}p < 0.01$, and $^{***}p < 0.001$.

3. Results

3.1. MP exposure inhibits the macrophage phagocytic activity

Morphology and size of PS-MPs were determined via field-emission scanning electron microscopy. As shown in Fig. 1, monodisperse MPs were spherical, with an average particle size of 0.1 μm. These MPs were used for subsequent tests. Next, we assessed the effects of MPs on macrophage viability. MTT assay was performed to evaluate the RAW264.7 cell viability after exposure to various MP concentrations (0, 20, 100, and 1000 μg/mL) for 24 h. No significant reduction in macrophage survival was observed (Fig. 2A). Notably, MPs did not affect pneumococcal viability (Fig. 2B). Overall, MPs did not affect both macrophage survival and pneumococcus viability.

We also investigated whether MPs influence the phagocytic activity of macrophages. Exposure of RAW264.7 cells to a low concentration of MPs (20 μg/mL) resulted in an approximately 50 % reduction in the uptake of FITC-labeled latex beads ($p = 0.0179$) (Fig. 3A, B). Phagocytic activity further declined with high MP concentrations at 100 μg/mL ($p = 0.0022$) and 1000 μg/mL ($p = 0.0020$). To evaluate the effect of MPs on pneumococcal engulfment, a gentamicin protection assay was performed. As shown in Fig. 3C, pneumococcal internalization by macrophages decreased progressively with increasing MP concentrations, with significant reductions observed at 20 μg/mL ($p = 0.00048$), 100 μg/mL ($p = 0.00004$), and 1000 μg/mL ($p = 0.00001$) compared with the control group. These findings suggest that MP exposure significantly impairs phagocytic activity and markedly hinders pneumococcal internalization by macrophages.

3.2. MPs synergistically aggravate the pneumococcus-induced inflammatory responses of macrophages

Next, the effects of MPs on inflammatory responses were assessed. Cytokine array assay was performed to compare the RAW264.7 cells treated with MPs and pneumococcus (MPs + Sp) to those treated with pneumococcus alone (Sp). As shown in Fig. 4, macrophages in the MPs + pneumococcus co-treatment group exhibited increased expression of intercellular adhesion molecule (ICAM)-1, CCL2, CXCL10, IL-1 receptor antagonist (IL-1ra), granulocyte-macrophage colony-stimulating factor (GM-CSF), CCL5, IL-6, CXCL12, and CCL4, and lower levels of CXCL2, TNF-α, G-CSF, and CCL3 than those in the pneumococcus alone group.

Similarly, mRNA expression analysis revealed significantly elevated *ICAM-1* ($p = 0.0002$), *CCL2* ($p = 0.0023$), and *GM-CSF* ($p = 0.0045$) in the MPs + pneumococcus co-treatment group compared to the

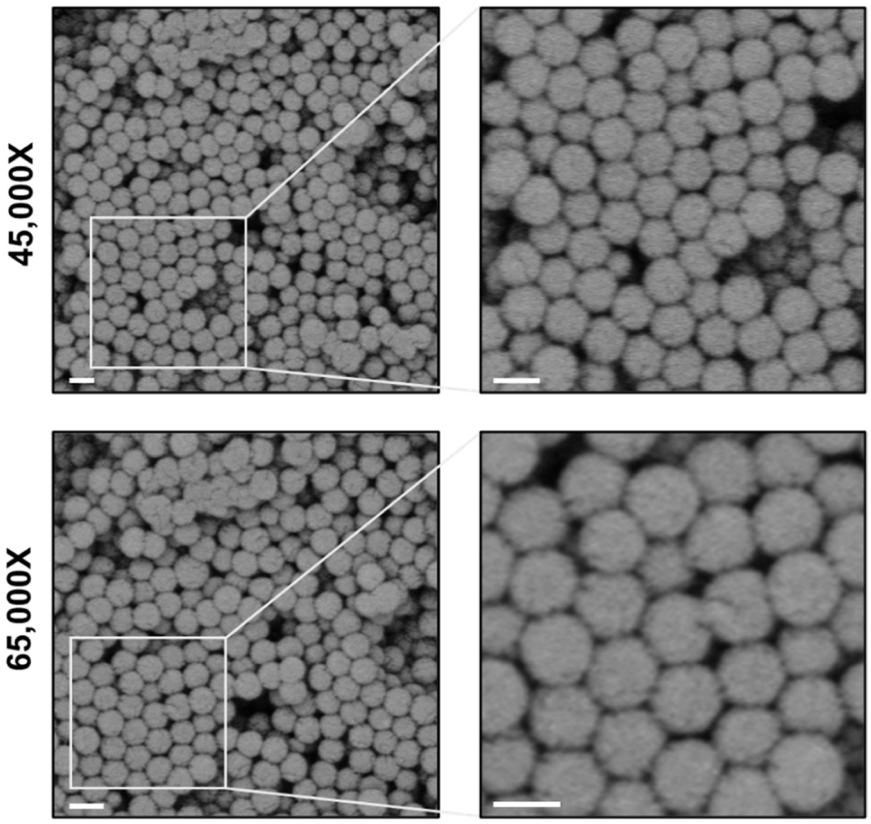

Fig. 1. Characterization of polystyrene-based MPs (PS-MPs). Morphology and size of PS-MPs were determined using a field-emission scanning electron microscope (FE-SEM). Magnified images of the cropped areas were shown in the right panels. Magnification of the graphs: 45,000 × (upper panels) and 65,000 × (lower panels). Scale bars, 100 nm.

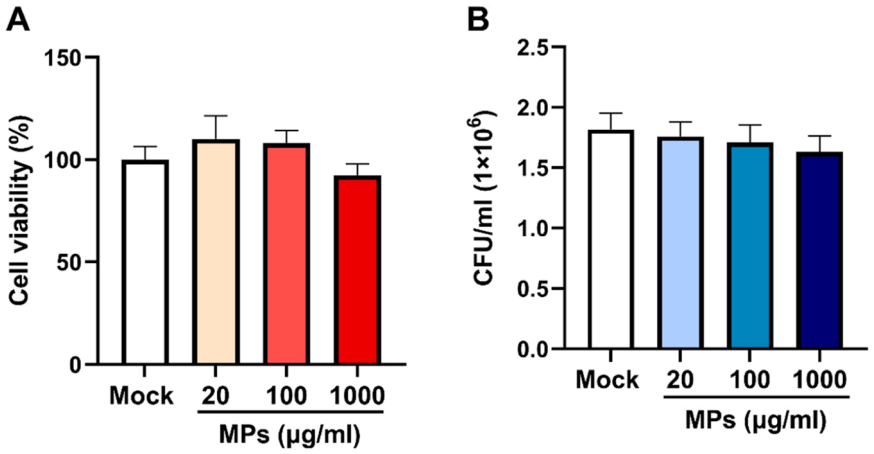

Fig. 2. MPs barely affect macrophage viability and pneumococcal survival. (A) RAW264.7 cells were exposed to various concentrations of MPs (0, 20, 100, and 1000 μg/mL) for 24 h, and cell viability was assessed using the 3-(4,5-dimethylthiazol-2-yl)-2,5-diphenyltetrazolium bromide (MTT) assay (n = 3). (B) Pneumococci were incubated with different concentrations of MPs for 6 h, and bacterial survival was determined by counting colony-forming units (CFU) on blood agar plates. Results represent the mean ± standard deviation from three independent experiments.

pneumococcus alone group, whereas no significant changes were observed in *CXCL10* and *IL-1ra* (Fig. 5). To validate these findings, cytokine production was quantified using ELISA. Secretion levels of CCL2 and CXCL10 were the highest in the MPs + pneumococcus co-treatment group, with CCL2 levels significantly higher than those in the pneumococcus alone group ($p = 0.0281$) (Fig. 6). Furthermore, levels of the pro-inflammatory cytokines, TNF-α ($p = 0.0181$) and IL-1α ($p = 0.0092$), were markedly elevated upon co-exposure to MPs and pneumococcus compared to the pneumococcus alone group (Figure S2). These results indicate that MPs enhance pneumococcus-induced cytokine production, exacerbating the inflammatory responses to bacterial infections.

3.3. MPs regulate the pneumococcus-induced inflammatory responses of macrophages via the PI3K/Akt and MAPK pathways

Luciferase assay was performed to assess the effects of MPs on NF-κB activity, which regulates CCL2 expression [26]. As shown in Fig. 7A,

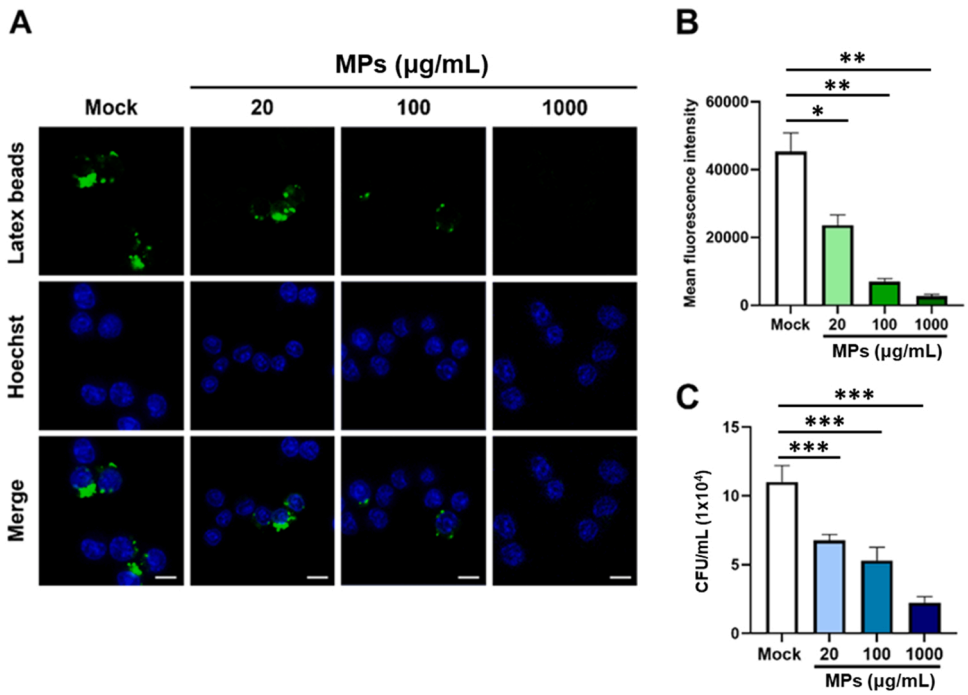

Fig. 3. MP exposure inhibits macrophage phagocytosis of pneumococci. (A) RAW264.7 cells were exposed to MPs at concentrations of 0, 20, 100, and 1000 μg/mL for 6 h, followed by incubation with fluorescein isothiocyanate (FITC)-labeled latex beads for 3 h. Nuclei were stained with Hoechst 33342, and images were captured using confocal microscopy and processed with ZEN software. Scale bars, 10 μm. (B) A total of 10 images were analyzed using ImageJ, and phagocytic activity was quantified based on the mean fluorescence intensity of internalized latex beads. (C) RAW264.7 cells were exposed to MPs (0, 20, 100, and 1000 μg/mL) for 24 h and then infected with pneumococci for 6 h. Intracellular bacterial survival was assessed using the gentamicin protection assay, and viable bacteria were quantified as colony-forming units (CFU). Results exhibit mean ± standard deviation from three independent experiments. Statistical significance was analyzed using one-way ANOVA followed by a post-hoc test. *, $p < 0.05$; **, $p < 0.01$; ***, $p < 0.001$.

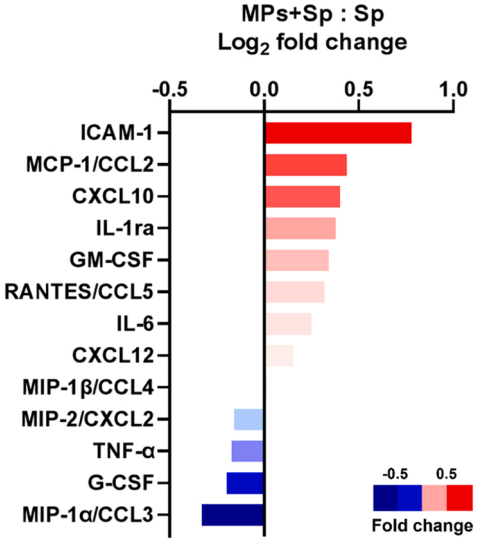

Fig. 4. Effects of MPs on pneumococcus-induced chemokine production in macrophages. RAW264.7 cells were exposed to 20 μg/mL MPs for 24 h and then infected with pneumococci at a multiplicity of infection (MOI) of 10 for 4 h. The levels of chemokines and cytokines were analyzed by cytokine array assay. Expression levels were quantified using UN-SCAN-IT graph digitizer software. The comparison between MPs + pneumococcus co-treatment and pneumococcus-only infection is represented as $\log_2$ fold changes (n = 2). Red indicates increased expression, whereas blue denotes decreased expression.

macrophages exposed to MPs alone showed no significant changes in NF-κB activity compared to those in the untreated group. In contrast, pneumococcal infection significantly increased the NF-κB activity ($p = 0.0159$), regardless of MP exposure. Notably, NF-κB activity in the MPs + pneumococcus co-treatment group was approximately twice as high as in the pneumococcus-infected macrophages without MP exposure ($p = 0.0005$).

We further examined the roles of MPs in CCL2-mediated inflammation in pneumococcus-infected macrophages. As shown in Fig. 7B, PI3K, phosphorylated Akt, and NF-κB subunit p65 levels were higher in the RAW264.7 cells co-treated with MPs and pneumococcus than in those infected with pneumococcus alone. Similarly, phosphorylation levels of p38, Erk, and JNK were markedly elevated in the MPs + pneumococcus co-treatment group (Fig. 7C). Collectively, these findings suggest that MP exposure followed by pneumococcal infection synergistically amplifies NF-κB activation in macrophages via CCL2-mediated activation of the PI3K/Akt and MAPK pathways.

3.4. *MPs affect pneumococcus-induced macrophage polarization*

To further examine the effects of MPs on macrophage polarization during pneumococcal infection, mRNA expression levels of M1/M2 macrophage markers were analyzed using qRT-PCR. Pneumococcal infection promoted M1 polarization, as evidenced by the increased gene expression of *CD80* ($p = 0.0004$) and inducible nitric oxide synthase (*iNOS*) ($p = 0.0002$) (Fig. 8). Remarkably, MP exposure enhanced the expression levels of M1 markers in the pneumococcus-infected macrophages. Conversely, mRNA expression of the anti-inflammatory M2 markers *CD163* ($p = 0.0053$) and *CD206* ($p = 0.00001$) was significantly lower in the MPs + pneumococcus co-treatment group than in the pneumococcus alone group. These findings suggest that MPs modulate pneumococcus-induced macrophage polarization, aggravating bacteria-induced inflammation.

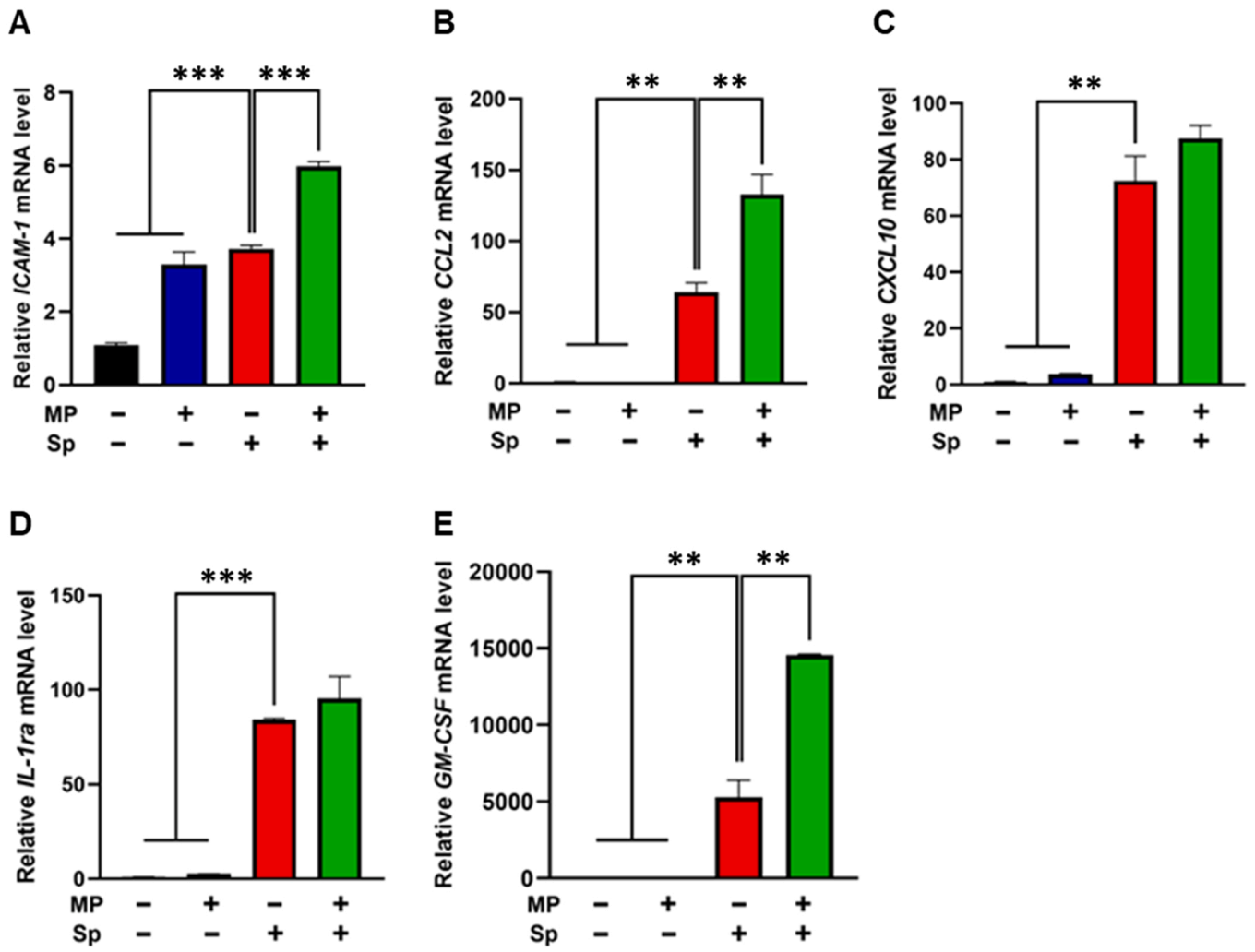

Fig. 5. MPs synergistically increase chemokine gene expression in pneumococcus-infected macrophages. RAW264.7 cells were exposed to 20 μg/mL MPs for 24 h, followed by pneumococcal infection at a multiplicity of infection (MOI) of 10 for 4 h. The mRNA expression levels of (A) *ICAM-1*, (B) *CCL2*, (C) *CXCL10*, (D) *IL-1ra*, and (E) *GM-CSF* were analyzed using qRT-PCR, with GAPDH as an internal control. Statistical significance was determined using one-way ANOVA followed by a post-hoc test. **, $p < 0.01$; ***, $p < 0.001$ (n = 4). CCL2, C-C motif chemokine ligand 2; CXCL10, C-X-C motif chemokine ligand 10; IL-1ra, interleukin-1 receptor antagonist; GAPDH, glyceraldehyde-3-phosphate dehydrogenase; GM-CSF, granulocyte-macrophage colony-stimulating factor; ICAM-1, intercellular adhesion molecule 1.

3.5. Co-exposure to MPs and pneumococcus synergistically promotes ROS generation and triggers ferroptosis in macrophages

Oxidative stress induces inflammatory responses by promoting the release of cytokines and chemokines and triggering iron-dependent cell death, known as ferroptosis [27]. Here, intracellular ROS production in pneumococcus-infected macrophages was significantly elevated and further amplified upon MP exposure ($p = 0.027$) (Fig. 9A). Additionally, lipid peroxidation, another hallmark of ferroptosis, was increased in the macrophages treated with MPs and pneumococcus compared to the untreated group (Figure S3). We then employed Ferrostatin-1, a specific ferroptosis inhibitor, to validate the involvement of ferroptosis in the observed macrophage cell death following co-treatment with MPs and pneumococcus. As shown in Figure S4, Ferrostatin-1 treatment significantly suppressed iron accumulation and subsequent cell death by co-treating with MPs and pneumococcus, supporting the conclusion that ferroptosis plays a major role in this context.

To investigate ferroptosis regulation, we analyzed key factors, including p53, the cystine antiporter SLC7A11 (xCT), and GPX4. p53 levels were markedly higher in the MPs + pneumococcus co-treatment group than in the MPs and pneumococcus alone groups (Fig. 9B). Additionally, pneumococcal infection, alone or in combination with MPs, downregulated the expression of xCT, a transporter involved in cystine uptake and glutathione synthesis, which plays a crucial role in ferroptosis regulation. Furthermore, co-treatment with MPs and pneumococcus led to reduced GPX4 levels compared to those in the untreated macrophages. An increase in p53 levels inhibits the cysteine transporter activity and reduces glutathione synthesis and GPX4 levels, thereby promoting ferroptosis [28]. These findings suggest that MPs enhance pneumococcus-induced ferroptosis by upregulating p53 levels and downregulating GPX4 and xCT levels.

3.6. MP exposure affects iron metabolism in pneumococcus-infected macrophages

Iron induces oxidative stress by increasing ROS production [29]. To determine whether MPs influence intracellular iron metabolism, we examined the levels of iron and its metabolism-related molecules. As shown in Fig. 10A–B, fluorescence microscopy revealed that MPs enhanced pneumococcus-induced iron accumulation in macrophages ($p = 0.0034$). Additionally, all treatment groups (MPs alone, pneumococcus alone, and MPs + pneumococcus) exhibited lower FTH1 levels

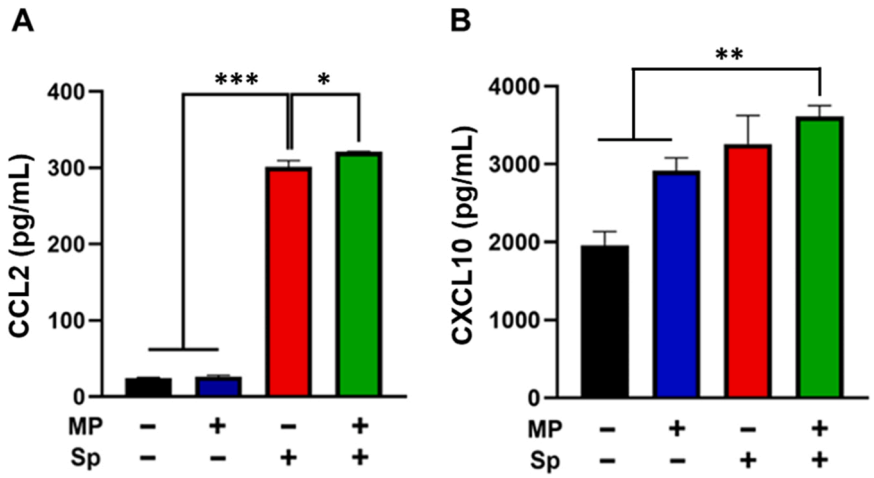

Fig. 6. MPs enhance pneumococcus-induced chemokine production in macrophages. RAW 264.7 cells were exposed to 20 μg/mL MPs for 24 h and then infected with pneumococci for an additional 4 h. The expression levels of (A) CCL2 and (B) CXCL10 were measured using enzyme-linked immunosorbent assay (ELISA). Statistical significance was determined using one-way ANOVA followed by a post-hoc test. *, $p < 0.05$; **, $p < 0.01$; ***, $p < 0.001$ (n = 3). CCL2, C-C motif chemokine ligand 2; CXCL10, C-X-C motif chemokine ligand 10.

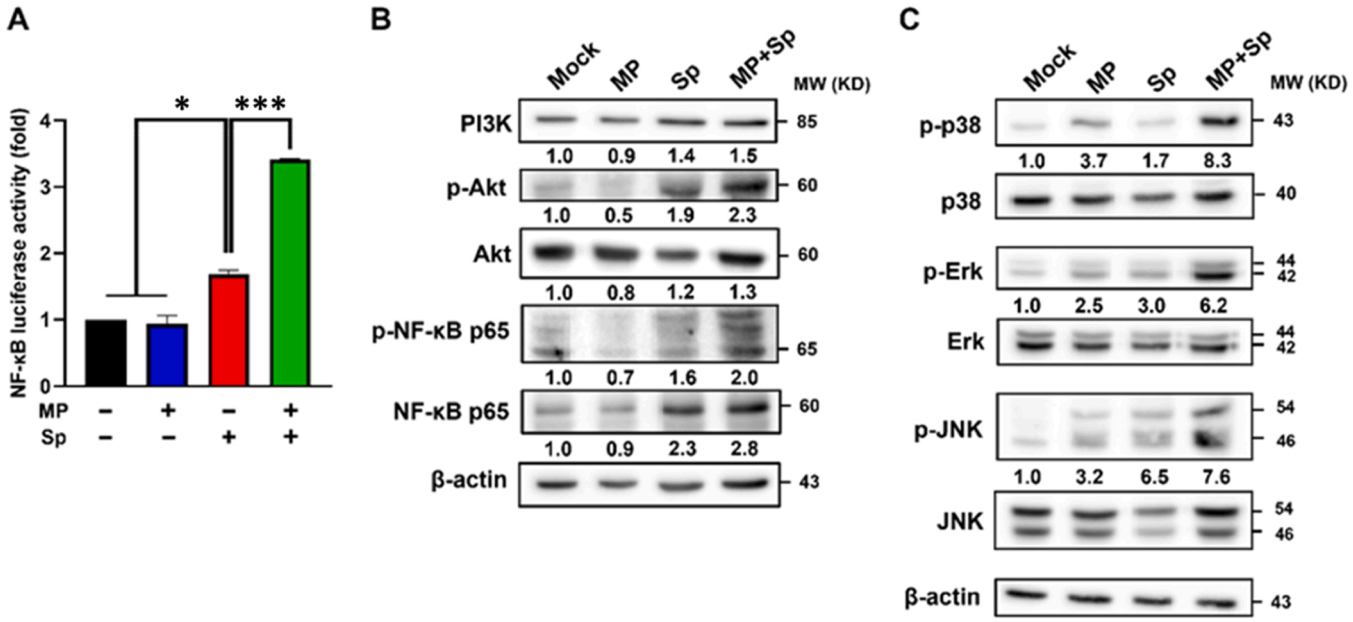

Fig. 7. MPs enhance pneumococcus-induced NF-κB activation through the PI3K/Akt and MAPK pathways in macrophages. (A) RAW 264.7 cells were transfected with an NF-κB luciferase reporter plasmid for 24 h, followed by treatment with MPs for 24 h and pneumococcal infection for 4 h. NF-κB luciferase activity was measured using the Dual-Luciferase Reporter Assay System. Statistical significance was determined using one-way ANOVA followed by a post-hoc test. *, $p < 0.05$; ***, $p < 0.001$ (n = 4). RAW 264.7 cells were treated with 20 μg/mL MPs for 24 h and infected with pneumococci for 4 h. Protein expression in cell lysates was analyzed via western blot assay using specific antibodies against (B) PI3K, Akt, phosphorylated Akt, NF-κB p65, and phosphorylated NF-κB p65, and (C) p38, Erk, JNK, and their respective phosphorylated forms. β-actin served as a loading control. Relative expression levels were normalized to mock-treated cells and are indicated under the respective lanes. Akt, protein kinase B; ERK, extracellular signal-regulated kinase; JNK, c-Jun N-terminal kinase; MAPK, mitogen-activated protein kinase; NF-κB, nuclear factor kappa-light-chain-enhancer of activated B cells; PI3K, phosphoinositide 3-kinase.

than the untreated group (Fig. 10C). Notably, NCOA4 levels were elevated following exposure to MPs and pneumococcus. These findings suggest that MPs and pneumococcal infection reduce iron storage and promote ferroptosis via NCOA4 in macrophages.

4. Discussion

Plastic particles are broadly categorized based on size into microplastics (MPs), defined as particles ranging from 1 μm to 5 mm, and nanoplastics (NPs), defined as particles smaller than 1 μm [30]. Given their overlapping environmental presence and biological effects, the collective term micro- and nanoplastics (MNPs) is increasingly used to encompass both size classes [31,32]. MPs are found in almost all ecosystems, with their global mass estimated to reach over one billion tons by 2060 [33]. These particles can enter the human body through various routes, including ingestion, inhalation, and dermal absorption [34]. Among these, inhalation is considered a primary exposure pathway, as MPs have been widely detected in pulmonary tissues [35,36]. Their effects on the respiratory system include lung injury, chronic inflammation, and oxidative stress [37].

Macrophages, dendritic cells, and neutrophils play critical roles as the first line of defense in innate immune responses. However, MPs can

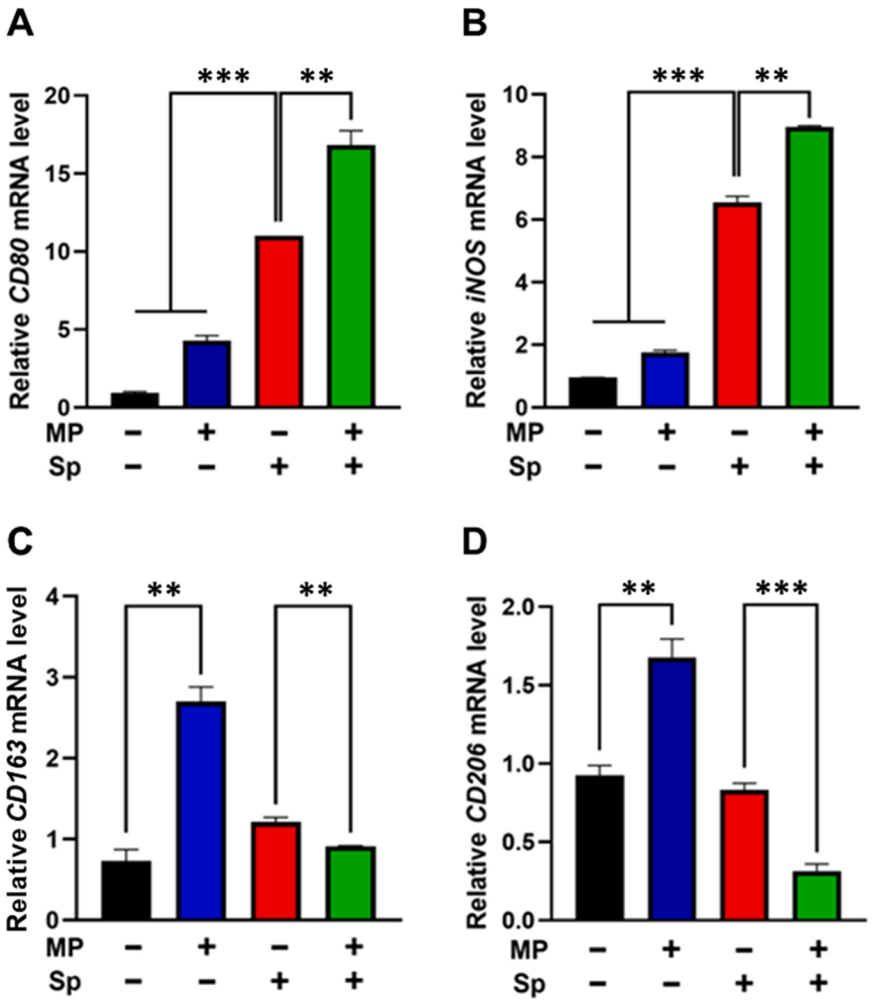

Fig. 8. MPs modulate pneumococcus-induced macrophage polarization. RAW 264.7 cells were treated with 20 μg/mL MPs for 24 h, followed by pneumococcal infection at a multiplicity of infection (MOI) of 10 for 4 h. The mRNA expression levels of M1 markers (A) *CD80* and (B) *iNOS*, and M2 markers (C) *CD163* and (D) *CD206* were analyzed using qRT-PCR, with glyceraldehyde-3-phosphate dehydrogenase (GAPDH) as an internal control. Statistical significance was determined using one-way ANOVA followed by a post-hoc test. **, $p < 0.01$; ***, $p < 0.001$. (n = 4). iNOS, inducible nitric oxide synthase.

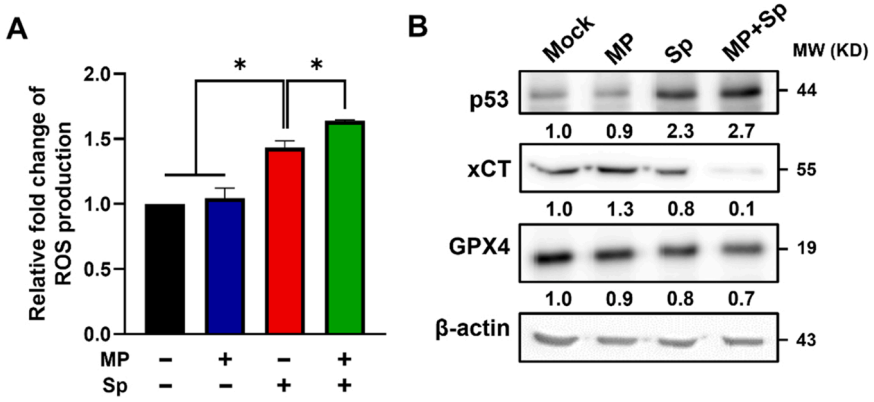

Fig. 9. MPs enhance ROS production and induce ferroptosis in pneumococcus-infected macrophages. (A) RAW 264.7 cells were treated with MPs for 24 h and then infected with pneumococci at a multiplicity of infection (MOI) of 10 for 2 h. Cells were stained with 10 μM dihydrorhodamine 123 (DHR123) and analyzed for intracellular ROS levels by flow cytometry. Statistical significance was determined using one-way ANOVA followed by a post-hoc test. *, $p < 0.05$ (n = 3). (B) RAW 264.7 cells were exposed to MPs for 24 h, followed by pneumococcal infection for 6 h. Cell lysates were analyzed by western blot assay for ferroptosis-related proteins, including p53, xCT, and GPX4. β-actin served as a loading control. Relative expression levels were normalized to those of mock-treated cells and are indicated under the respective lanes. GPX4, glutathione peroxidase 4; ROS, reactive oxygen species; xCT, cystine/glutamate transporter.

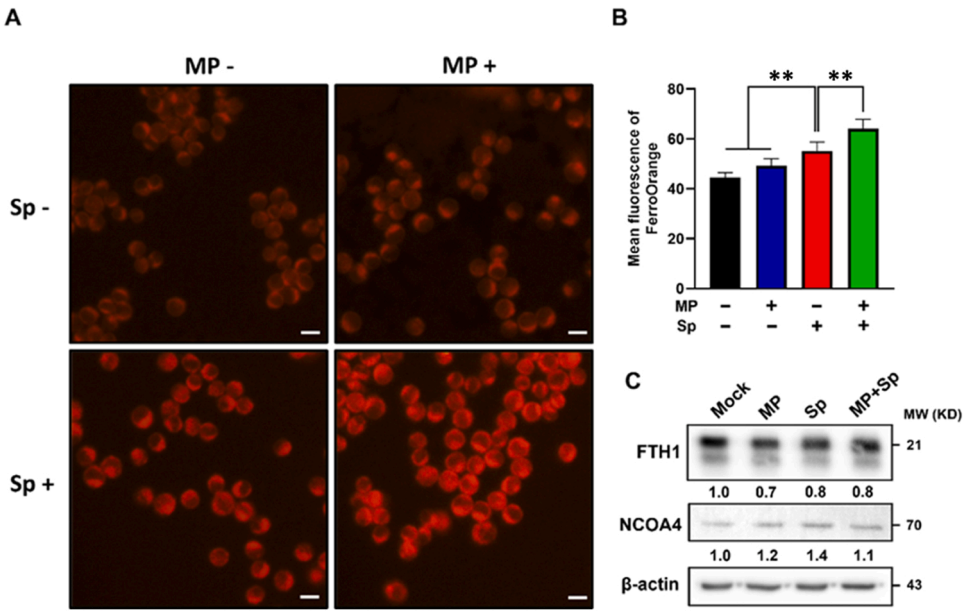

Fig. 10. MPs elicit iron metabolism and induce ferroptosis in pneumococcus-challenged macrophages. RAW 264.7 cells were treated with MPs for 24 h and then infected with pneumococci at a multiplicity of infection (MOI) of 10 for 6 h. (A) Intracellular iron levels were visualized using FerroOrange (1 μmol/L) and analyzed by fluorescence microscopy. Scale bars, 10 μm. (B) Quantification of intracellular iron levels based on the mean fluorescence intensity of FerroOrange. (C) Western blot analysis of FTH1 and NCOA4 expression levels. Relative protein expression was normalized to mock-treated cells and indicated below each lane. Statistical significance was determined using one-way ANOVA followed by a post-hoc test. **, $p < 0.01$. FTH1, ferritin heavy chain 1; NCOA4, nuclear receptor coactivator 4.

be internalized by macrophages, which induce toxicity depending on their physicochemical properties, including size, concentration, and the duration of exposure (44). Smaller particle sizes, irregular morphologies, higher concentrations, and prolonged exposure have all been shown to amplify adverse effects in both animals and humans. Additionally, recent evidence suggests that MPs can interfere with microbial uptake processes, such as bacterial endocytosis, potentially disrupting immune regulation in various organisms, including soil invertebrates (45). The increasing global prevalence of MPs is detrimental to living animals, and their presence in different tissues is harmful to human health. In this study, we investigated the effects of MPs on macrophage function during pneumococcal infection, aiming better to understand their potential role in modulating host immune responses.

Previous studies have estimated that humans typically inhale between 6.50 and 8.97 μg of MPs per kilogram of body weight per day, with exposure levels reported to be 3–50 times higher in infants and preschool-aged children [38]. The lungs have been identified as a major site of MP accumulation, with estimated burdens reaching 34–35 mg, corresponding to approximately 10,728–11,317 particles per individual [39]. In certain regions, such as China and Mongolia, daily inhalation of MPs may be as high as 2.85×10^6 particles per adult [40]. Occupational exposure, particularly among individuals working in the plastic manufacturing industry, is likely to be even greater, although comprehensive data remain limited. In this study, we assessed macrophage viability across a range of MP concentrations and found that even at doses as high as 1000 μg/mL, MPs did not significantly reduce cell survival. These findings suggest that macrophages can tolerate relatively high levels of MP exposure without undergoing overt cytotoxicity. Considering the variability in real-world exposure levels and the observed resilience of macrophages, we selected a concentration of 20 μg/mL to investigate the effects of MPs on pneumococcus-induced inflammation. The dose was chosen to reflect environmentally relevant exposure scenarios and to explore the potential immunomodulatory effects of MPs under infectious conditions.

Pneumococcus typically colonizes the nasopharynx asymptomatically, particularly in healthy individuals. However, it can transition to a pathogenic state, causing invasive diseases such as pneumonia, sepsis, and meningitis, especially in children under five years of age [4]. Our results showed that PS-MPs significantly inhibited bacterial phagocytosis and impaired pneumococcal clearance, exacerbating inflammatory responses during infection. Other polymer types, such as PE-MPs, have also been reported to impair macrophage phagocytic function [41]. Moreover, polymers like PE-MPs and PVC-MPs often contain residual monomers or chemical additives, which may elicit stronger inflammatory and cytotoxic responses than more inert polymers such as PS-MPs [42]. Further, NPs (< 100 nm) generally exhibit greater cellular internalization efficiency than larger MPs, owing to their smaller size and higher surface area-to-volume ratio [16]. These differences can lead to enhanced oxidative stress, inflammation, and genotoxicity of immune cells. Future studies should explore a broader range of particle sizes and polymer types to better understand the diverse biological impacts of MPs under physiologically relevant conditions.

In this study, macrophages exhibited upregulated mRNA levels of cytokines and chemokines, including *ICAM-1*, *CCL2*, *GM-CSF*, *CXCL10*, and *IL-1Ra*, in response to pneumococcal infection. MPs increased the *ICAM-1*, *CCL2*, and *GM-CSF* mRNA levels upon co-treatment with pneumococcus. MPs also promoted the production of cytokines and chemokines, including CCL2, CXCL10, TNF-α, IL-1α, and IL-1β, in the infected macrophages. Specifically, CCL2, TNF-α, and IL-1α levels were significantly elevated due to the synergistic effects of MPs and pneumococcal infection. These findings suggest that MP exposure enhances the innate immune responses during pneumococcal infection, exacerbating the pro-inflammatory responses and contributing to chronic inflammation.

CCL2 recruits macrophages to the sites of inflammation and bacterial infection by promoting adhesion, migration, and intracellular signaling, leading to macrophage activation, ROS production, and M1-type polarization. In this study, CCL2 production was significantly higher in the MPs + pneumococcus co-treatment group than in the MP exposure and pneumococcal infection alone groups. Additionally, MPs induced CCL2-mediated activation of the PI3K/Akt, MAPK, and NF-κB signaling pathways during pneumococcal infection, regulating gene expression and promoting immune mediator production in macrophages. NF-κB activation is essential for macrophage differentiation into the pro-

inflammatory M1 phenotype [43]. Consistently, we observed significant upregulation of the levels of M1 macrophage biomarkers, including *CD80* and *iNOS*, in the MPs + pneumococcus co-treatment group. Consequently, activated macrophages secreted high levels of pro-inflammatory cytokines, including TNF-α, IL-1α, and IL-1β. These results suggest that CCL2 plays a critical role in macrophage activation, contributing to the host defense against MPs and exacerbating the inflammatory responses during pneumococcal infection.

Ferroptosis is a recently identified form of regulated cell death characterized by iron overload and lipid peroxidation [44]. In this study, macrophages co-treated with MPs and pneumococcus showed significantly upregulated ROS production compared to the other treatment groups (untreated, MPs alone, and pneumococcus alone). MP exposure elevates the levels of ROS and mitochondrial deacetylase sirtuin 3 (SIRT3), a key regulator of ROS production, in mouse hepatocytes [45]. Iron is essential for various cellular processes but contributes to oxidative damage when present in excess or in a dysregulated state [28,44]. Under iron-rich conditions, FTH1 captures and stores the iron ions in ferritin complexes, preventing their involvement in ROS-generating reactions [46]. Ferrostatin-1 treatment effectively attenuated iron accumulation and suppressed ferroptosis-associated cell death induced by the co-treatment of macrophages with MPs and pneumococcus. Consistently, we found that macrophages co-treated with MPs and pneumococcus exhibited high iron levels and low FTH1 expression levels, which exacerbated the inflammatory responses during infection.

Although this study provides important insights into how MPs impair macrophage responses to pneumococcal infection, several limitations should be noted. The use of an *in vitro* macrophage model, while informative, does not fully replicate the complexity of the human immune system or lung environment. Additionally, we focused on a single type of synthetic PS-MPs with uniform size and shape, which may not reflect the diverse physicochemical properties of environmental MPs. Real-world MPs vary in composition, size, and shape, all of which can influence their biological effects. Furthermore, potential interactions between MPs and bacterial cells, such as aggregation or changes in bacterial infectivity, warrant further investigation. Finally, the absence of clinical or epidemiological data limits the translational applicability of our findings. Future studies should include patient-derived samples, particularly from individuals in MP-polluted areas, to better understand the real-world implications of MP exposure on respiratory infections.

5. Conclusions

In conclusion, MP exposure inhibited macrophage functions, impaired bacterial clearance, and exacerbated pneumococcus-induced inflammation (Fig. 11). Additionally, MPs disrupted macrophage polarization and promoted dysfunction through CCL2-mediated activation of the PI3K/Akt and NF-κB signaling pathways. Furthermore, MP and pneumococcus co-exposure synergistically elevated ROS production and disrupted iron homeostasis, thereby driving ferroptosis. These findings provide crucial insights into the mechanisms how MPs exacerbate pneumococcal infection and highlight the need for targeted therapies to mitigate MP-induced immune dysregulation in respiratory infections.

Environmental implication

The widespread presence of MPs in the environment poses a significant risk to respiratory health by impairing macrophage functions, reducing bacterial clearance, and exacerbating pneumococcus-induced inflammation. Our findings show that MP exposure dampens macrophage defenses through the modulation of inflammatory signaling pathways and ferroptosis, increasing susceptibility to pneumococcal infections. Given the rising levels of MP pollution, reducing human exposure through stricter environmental regulations and pollution control measures is essential. These insights highlight the need for further research and policy interventions to mitigate the health impacts of MPs.

Funding

This study was supported by the National Science and Technology Council (112-2320-B-182-036-MY3, 112-2320-B-182-042-MY3, 113-2321-B-182A-004), Chang Gung Memorial Hospital (CMRPD1L0321, CMRPD1M0491-2, and CORPD1M0021-3, and CMRPD1P0161), Research Center for Emerging Viral Infections from the Featured Areas Research Center Program within the framework of the Higher Education Sprout Project by the Taiwan Ministry of Education, and Tomorrow Medical Foundation

CRediT authorship contribution statement

Ko-Wei Chang: Writing – original draft, Investigation. **Jo-Tsen Chen:** Writing – original draft, Investigation, Data curation. **Chun-Ning**

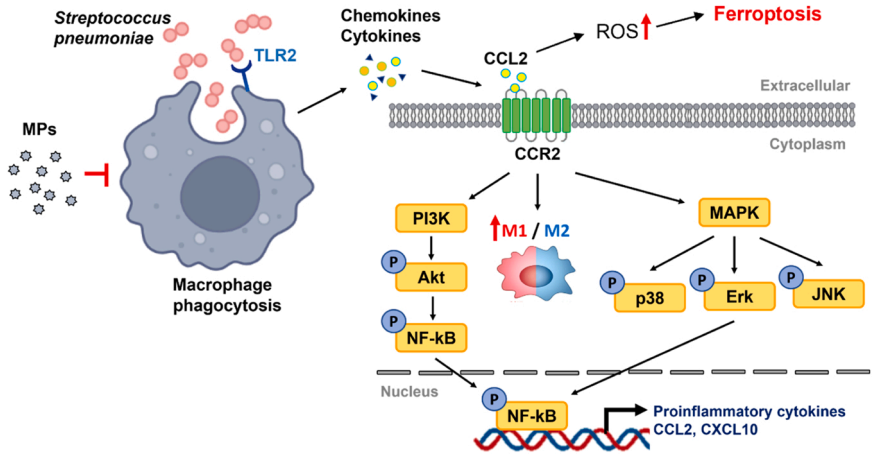

Fig. 11. A schematic model illustrating the underlying mechanism of MPs exacerbates pneumococcus-induced macrophage inflammation. MP exposure reduces macrophage phagocytic activity, leading to impaired pneumococcal clearance during infection. Additionally, MPs amplify pneumococcus-induced chemokine production by activating the PI3K/Akt and MAPK pathways, promoting M1 macrophage polarization. Furthermore, the combined effects of MPs and pneumococcal infection synergistically enhance reactive oxygen species (ROS) production, ultimately inducing ferroptosis in macrophages. Akt, protein kinase B; ERK, extracellular signal-regulated kinase; JNK, c-Jun N-terminal kinase; MAPK, mitogen-activated protein kinase; NF-κB, nuclear factor kappa-light-chain-enhancer of activated B cells; PI3K, activation through the phosphoinositide 3-kinase.

Chuang: Writing – original draft, Data curation. **Ming-Ling Kuo:** Supervision, Conceptualization. **Kuo-Chin Kao:** Supervision, Conceptualization. **Cheng-Hsun Chiu:** Validation, Conceptualization. **Chih-Ho Lai:** Writing – review & editing, Validation, Conceptualization. **Dang Thi Thanh Thao:** Writing – original draft, Data curation. **Yu-Tsen Huang:** Investigation, Data curation. **Hui-Yu Wu:** Investigation, Data curation.

Declaration of Competing Interest

The authors declare that they have no known competing financial interests or personal relationships that could have appeared to influence the work reported in this paper.

Acknowledgments

The authors would like to thank the editor and reviewers for their editorial assistance and valuable comments. The authors sincerely appreciate assistance in analyzing confocal microscopy (Microscopy Center, Chang Gung University).

Appendix A. Supporting information

Supplementary data associated with this article can be found in the online version at doi:10.1016/j.jhazmat.2025.139696.

Data Availability

Data will be made available on request.

References

[1] Osman, A.I., Hosny, M., Eltaweil, A.S., et al., 2023. Microplastic sources, formation, toxicity and remediation: a review. Environ Chem Lett 1–41. https://doi.org/10.1007/s10311-023-01593-3.
[2] Rozman, U., Kalcikova, G., 2022. Seeking for a perfect (non-spherical) microplastic particle - the most comprehensive review on microplastic laboratory research. J Hazard Mater 424, 127529. https://doi.org/10.1016/j.jhazmat.2021.127529.
[3] Aras Kadioglu, J.N.W., Paton, James C., Andrew, Peter W., 2008. The role of streptococcus pneumoniae virulence factors in host respiratory colonization and disease. Nat Rev Microbiol 6, 288–301. https://doi.org/10.1038/nrmicro1871.
[4] Koppe, U., Suttorp, N., Opitz, B., 2012. Recognition of *streptococcus pneumoniae* by the innate immune system. Cell Microbiol 14, 460–466. https://doi.org/10.1111/j.1462-5822.2011.01746.x.
[5] Preston, J.A., Bewley, M.A., Marriott, H.M., et al., 2019. Alveolar macrophage Apoptosis-associated bacterial killing helps prevent murine pneumonia. Am J Respir Crit Care Med 200, 84–97. https://doi.org/10.1164/rccm.201804-0646OC.
[6] Dockrell, D.H., Marriott, H.M., Prince, L.R., et al., 2003. Alveolar macrophage apoptosis contributes to pneumococcal clearance in a resolving model of pulmonary infection. J Immunol 171, 5380–5388.
[7] Fueldner, C., Kohlschmidt, J., Riemschneider, S., et al., 2018. Benzo(a)pyrene attenuates the pattern-recognition-receptor induced proinflammatory phenotype of murine macrophages by inducing IL-10 expression in an aryl hydrocarbon receptor-dependent manner. Toxicology 409, 80–90. https://doi.org/10.1016/j.tox.2018.07.011.
[8] Kafka, D., Ling, E., Feldman, G., et al., 2008. Contribution of IL-1 to resistance to streptococcus pneumoniae infection. Int Immunol 20, 1139–1146. https://doi.org/10.1093/intimm/dxn071.
[9] Genin, M., Clement, F., Fattaccioli, A., Raes, M., Michiels, C., 2015. M1 and M2 macrophages derived from THP-1 cells differentially modulate the response of cancer cells to etoposide. BMC Cancer 15, 577. https://doi.org/10.1186/s12885-015-1546-9.
[10] Tamagawa, E., Bai, N., Morimoto, K., et al., 2008. Particulate matter exposure induces persistent lung inflammation and endothelial dysfunction. Am J Physiol Lung Cell Mol Physiol 295, L79–L85. https://doi.org/10.1152/ajplung.00048.2007.
[11] Palaniappan, S., Sadacharan, C.M., Rostama, B., 2022. Polystyrene and polyethylene microplastics decrease cell viability and dysregulate inflammatory and oxidative stress markers of MDCK and L929 cells in vitro. Expo Health 14, 75–85. https://doi.org/10.1007/s12403-021-00419-3.
[12] Liu, Y., Liu, W., Yang, X., et al., 2021. Microplastics are a hotspot for antibiotic resistance genes: progress and perspective. Sci Total Environ 773, 145643. https://doi.org/10.1016/j.scitotenv.2021.145643.
[13] Park, K.-M., Kim, B., Woo, W., Kim, L.K., Hyun, Y.-M., 2024. Polystyrene microplastics induce activation and cell death of neutrophils through strong adherence and engulfment. J Hazard Mater 480, 136100. https://doi.org/10.1016/j.jhazmat.2024.136100.
[14] A. F. R. M, Ramsperger, V.K, B.N., W, Gross, Mohanraj, J., Thelakkat, M., Greiner, A., Schmalz, H., Kress, H., Laforsch, C., 2020. Environmental exposure enhances the internalization of microplastic particles into cells. Sci Adv.
[15] Chen, J., Xu, Z., Liu, Y., et al., 2023. Cellular absorption of polystyrene nanoplastics with different surface functionalization and the toxicity to RAW264.7 macrophage cells. Ecotoxicol Environ Saf 252, 114574. https://doi.org/10.1016/j.ecoenv.2023.114574.
[16] Adler, M.Y., Issoual, I., Ruckert, M., et al., 2024. Effect of micro- and nanoplastic particles on human macrophages. J Hazard Mater 471, 134253. https://doi.org/10.1016/j.jhazmat.2024.134253.
[17] Luo, W.Q., Cao, M.T., Sun, C.X., et al., 2025. Size-dependent internalization of polystyrene microplastics as a key factor in macrophages and systemic toxicity. J Hazard Mater 490, 137701. https://doi.org/10.1016/j.jhazmat.2025.137701.
[18] Chen, Y., Fang, Z.-M., Yi, X., Wei, X., Jiang, D.-S., 2023. The interaction between ferroptosis and inflammatory signaling pathways. Cell Death Dis 14, 205. https://doi.org/10.1038/s41419-023-05716-0.
[19] Wang, Y., Quan, F., Cao, Q., et al., 2021. Quercetin alleviates acute kidney injury by inhibiting ferroptosis. J Adv Res 28, 231–243. https://doi.org/10.1016/j.jare.2020.07.007.
[20] Gschwandtner, M., Derler, R., Midwood, K.S., 2019. More than just attractive: how CCL2 influences myeloid cell behavior beyond chemotaxis. Front Immunol 10, 2759. https://doi.org/10.3389/fimmu.2019.02759.
[21] Tang, J., Bu, W., Hu, W., et al., 2023. Ferroptosis is involved in Sex-Specific small intestinal toxicity in the offspring of adult mice exposed to polystyrene nanoplastics during pregnancy. ACS Nano 17, 2440–2449. https://doi.org/10.1021/acsnano.2c09729.
[22] Wang, H., Hu, C., Li, Y., et al., 2024. Nano-sized polystyrene and magnetite collectively promote biofilm stability and resistance due to enhanced oxidative stress response. J Hazard Mater 476, 134974. https://doi.org/10.1016/j.jhazmat.2024.134974.
[23] Lee, H.Y., Wu, T.L., Su, L.H., et al., 2018. Invasive pneumococcal disease caused by ceftriaxone-resistant *streptococcus pneumoniae* in Taiwan. J Microbiol Immunol Infect 51, 500–509. https://doi.org/10.1016/j.jmii.2016.12.004.
[24] Chen, Y.W., Huang, M.Z., Chen, C.L., et al., 2020. PM2.5 impairs macrophage functions to exacerbate pneumococcus-induced pulmonary pathogenesis. Part Fibre Toxicol 17, 37. https://doi.org/10.1186/s12989-020-00362-2.
[25] Chou, Li-Fang, C, T.-W., Yang, Huang-Yu, Tian, Ya-Chung, Chang, Ming-Yang, Hung, Cheng-Chieh, Lai, Chih-Ho, Hsu, Shen-Hsing, Tsai, Chung-Ying, Ko, Yi-Ching, Lian, Jang-Hau, Yang, Chih-Wei, 2022. Implication of the IL-10-Expression signature in the pathogenicity of Leptospira-Infected macrophages. Microbiol Spectr 10.
[26] Deng, X., Xu, M., Yuan, C., et al., 2013. Transcriptional regulation of increased CCL2 expression in pulmonary fibrosis involves nuclear factor-kappaB and activator protein-1. Int J Biochem Cell Biol 45, 1366–1376. https://doi.org/10.1016/j.biocel.2013.04.003.
[27] Mu, Y., Sun, J., Li, Z., et al., 2022. Activation of pyroptosis and ferroptosis is involved in the hepatotoxicity induced by polystyrene microplastics in mice. Chemosphere 291, 132944. https://doi.org/10.1016/j.chemosphere.2021.132944.
[28] Tang, D., Chen, X., Kang, R., Kroemer, G., 2021. Ferroptosis: molecular mechanisms and health implications. Cell Res 31, 107–125. https://doi.org/10.1038/s41422-020-00441-1.
[29] Liu, X., Yang, H., Yan, X., et al., 2022. Co-exposure of polystyrene microplastics and iron aggravates cognitive decline in aging mice via ferroptosis induction. Ecotoxicol Environ Saf 233, 113342. https://doi.org/10.1016/j.ecoenv.2022.113342.
[30] Ali, I., Cheng, Q.H., Ding, T.D., et al., 2021. Micro- and nanoplastics in the environment: occurrence, detection, characterization and toxicity-A critical review (ARTN). J Clean Prod 313, 127863. https://doi.org/10.1016/j.jclepro.2021.127863.
[31] Rondon, R., Cardenas, C.A., Cosseau, C., et al., 2024. Physiological and molecular effects of contaminants of emerging concerns of micro and nano-size in aquatic metazoans: overview and current gaps in antarctic species. Environ Sci Pollut Res Int 31, 48888–48907. https://doi.org/10.1007/s11356-024-34457-6.
[32] Chen, Y., Jing, S., Wang, Y., et al., 2024. Quantification and characterization of fine plastic particles as considerable components in atmospheric fine particles. Environ Sci Technol 58, 4691–4703. https://doi.org/10.1021/acs.est.3c06832.
[33] Editorial, Microplastics are everywhere, 2024. We need to understand how they affect human health, 913 Nat Med 30, 913. https://doi.org/10.1038/s41591-024-02968-x.
[34] Winiarska, E., Jutel, M., Zemelka-Wiacek, M., 2024. The potential impact of nano- and microplastics on human health: understanding human health risks. Environ Res 251, 118535. https://doi.org/10.1016/j.envres.2024.118535.
[35] Amato-Lourenço, L.F., Carvalho-Oliveira, R., Júnior, G.R., et al., 2021. Presence of airborne microplastics in human lung tissue. J Hazard Mater 416, 126124. https://doi.org/10.1016/j.jhazmat.2021.126124.
[36] Jenner, L.C., Rotchell, J.M., Bennett, R.T., et al., 2022. Detection of microplastics in human lung tissue using μFTIR spectroscopy. Sci Total Environ 831, 154907. https://doi.org/10.1016/j.scitotenv.2022.154907.
[37] Chartres, N., Cooper, C.B., Bland, G., et al., 2024. Effects of microplastic exposure on human digestive, reproductive, and respiratory health: a rapid systematic review. Environ Sci Technol 58, 22843–22864. https://doi.org/10.1021/acs.est.3c09524.

[38] Dewika, M., Markandan, K., Irfan, N.A., et al., 2023. Review of microplastics in the indoor environment: distribution, human exposure and potential health impacts. Chemosphere 324, 138270. https://doi.org/10.1016/j.chemosphere.2023.138270.
[39] Zhu, L., Kang, Y., Ma, M., et al., 2024. Tissue accumulation of microplastics and potential health risks in human. Sci Total Environ 915, 170004. https://doi.org/10.1016/j.scitotenv.2024.170004.
[40] Zhao, X., You, F., 2024. Microplastic human dietary uptake from 1990 to 2018 grew across 109 major developing and industrialized countries but can be halved by plastic debris removal. Environ Sci Technol 58, 8709–8723. https://doi.org/10.1021/acs.est.4c00010.
[41] Jasinski, J., Volkl, M., Wilde, M.V., et al., 2024. Influence of the polymer type of a microplastic challenge on the reaction of murine cells. J Hazard Mater 465, 133280. https://doi.org/10.1016/j.jhazmat.2023.133280.
[42] Yang, W., Jannatun, N., Zeng, Y., et al., 2022. Impacts of microplastics on immunity. Front Toxicol 4, 956885. https://doi.org/10.3389/ftox.2022.956885.
[43] Guo, Q., Jin, Y., Chen, X., et al., 2024. NF-κB in biology and targeted therapy: new insights and translational implications. Signal Transduct Target Ther 9, 53. https://doi.org/10.1038/s41392-024-01757-9.
[44] Zhang, C., Liu, X., Jin, S., Chen, Y., Guo, R., 2022. Ferroptosis in cancer therapy: a novel approach to reversing drug resistance. Mol Cancer 21, 47. https://doi.org/10.1186/s12943-022-01530-y.
[45] Zou, H., Qu, H., Bian, Y., et al., 2023. Polystyrene microplastics induce oxidative stress in mouse hepatocytes in relation to their size. Int J Mol Sci 24. https://doi.org/10.3390/ijms24087382.
[46] Ito, J., Omiya, S., Rusu, M.C., et al., 2021. Iron derived from autophagy-mediated ferritin degradation induces cardiomyocyte death and heart failure in mice. Elife 10. https://doi.org/10.7554/eLife.62174.